Fluid flow in a microfluidic paper-based porous substrate by capillary action

Samira Allameh
university of isfahan https://orcid.org/0000-0002-8787-1372
Mohsen Rabbani (m.rabbani@eng.ui.ac.ir)
university of isfahan https://orcid.org/0000-0002-9187-076X
Mahmood Reza Sadeghi
university of isfahan

Research Article

Keywords: Two-phase flow, Capillary action, Porous structure, ANSYS fluent

Posted Date: April 14th, 2022

DOI: https://doi.org/10.21203/rs.3.rs-1557529/v1

Fluid flow in a microfluidic paper-based porous substrate by capillary action

Samira Allameh[a], Mohsen Rabbani[b*], Mahmood Reza Sadeghi[c]

[a] Department of Biomedical Engineering, Faculty of Engineering, University of Isfahan, Isfahan, Iran, https://orcid.org/0000-0002-8787-1372

[b] Department of Biomedical Engineering, Faculty of Engineering, University of Isfahan, Isfahan, Iran, *https://orcid.org/0000-0002-9187-076X*

[c] Department of Biomedical Engineering, Faculty of Engineering, University of Isfahan, Isfahan, Iran

[*] Corresponding author, Azadi Sq. Isfahan, Iran, 81746-73441, Tel: +983137935627, Email: m.rabbani@eng.ui.ac.ir

Abstract

Paper has a porous structure, and fluid imbibition in a paper channel is possible passively through the hydrophilic surfaces by capillary action, so it can be an appropriate substrate in the field of microfluidics. To realize the fluid behavior in a paper-based microchannel, there is a need to obtain a model for fluid flow. In this study, the capillary-driven flow in a porous structure was simulated, and the effect of geometrical and physical parameters on the wetted length and average fluid pressure was investigated. Geometric parameters are pores' shape and size, channel dimensions, and porosity, while the investigated physical parameters were the contact angle, surface tension coefficient, and viscosity. According to the results, geometric parameters influenced the capillary pressure through the capillary surface and channel resistance variation, and physical parameters directly impacted the capillary pressure. Considering the wetted length results, the fluid imbibition velocity was fast at the beginning of the simulation and reached a constant value over time due to the increase in the flow resistance. The pressure drop was observed in the liquid phase suggesting the fluid flow from the higher pressure to lower. The wetted-length equation was obtained based on geometrical and physical parameters. Finally, the proposed equation can be used to design and predict the liquid imbibition in porous channels.

Keywords: Two-phase flow; Capillary action; Porous structure; ANSYS fluent

Acknowledgments

The team acknowledges the generous funding provided by the University of Isfahan, Isfahan, Iran.

1. Introduction

1.1. Theory

Controlling the fluid flow is essential both in passive and active microfluidic systems. Flows arising from the capillarity are influenced by the chemical and physical properties of the fluid phase's interface and geometric features of the channel [1, 2]. Recently, the paper material has attracted the attention of researchers as the substrate in the field of microfluidics and is used for environmental monitoring, clinical and health diagnosis, and food quality control [3, 4]. Paper is produced by compressing cellulose fibers and has a porous structure [5, 6]. Filter paper with a randomized arrangement of fibers is one of the standard papers for diagnostic application [7, 8]. Paper has various advantages such as the low cost, producible in different scales and sizes, removal of the bubble-associated problems, and the most crucial feature, fluid wicking passively through the capillary action [3, 6, 8, 9].

According to World Health Organization (WHO) instruction for the fabrication of microfluidic paper-based analytical device (μPAD), an appropriate μPAD for diagnosis application should be ASSURED (which stands for affordability, sensitivity, specificity and selectivity, being user-friendly, rapid and robust, equipment-free, and deliverable to the end-users). Thus, for the fabrication of an ASSURED diagnostic μPAD, mathematical modeling is required to predict the fluid flow [5, 10]. The paper structure in microscale is complex because it has a randomized porous structure, and the fluid flow can occur by capillarity. Based on Washburn's equation for capillary flow and Darcy's law for a porous structure, mathematical modeling was utilized to predict fluid imbibition in a paper-based channel [5]. Therefore, both Washburn and Darcy's modeling should be used to predict fluid flow in a paper-based channel.

In various studies, the fluid flow in porous media was investigated through numerical and experimental methods. Ashari numerically solved nonlinear equations for fluid flow in porous media utilizing Darcy's law by considering saturation [11]. Another study investigated the fluid flow in porous media for moving and stationary walls [12]. Lagree solved the equations for porous media with the finite volume method (FVM) modeling [13]. Cai et al. solved mass equations using FVM [14]. In another study, the capillary-driven flow was investigated for a rectangular channel by assuming the transient velocity (instead of the developed flow assumption) for the capillary action in a rectangular microchannel [15, 16]. In another sudy, the equation was solved in a microchannel by assuming the slip condition on one of the walls [17].

The effect of inertia in Navier-Stokes equations in a capillary-driven flow was considered in other studies [18, 19]. Songok et al. obtained a time-dependent power-law equation for the wetted length, experimentally [3]. Elizalde et al. proposed a model for inconstant cross-sections based on Washburn's equation [8]. In addition, Liu et al. proposed equations by considering the effect of evaporation numerically and experimentally [9]. In another study, the effect of contact angle (CA) was investigated [20]. Schaumburg and Berli solved Washburn's equation for a multilayer paper-based device [21]. The summary of the recent studies is presented in **Error! Reference source not found.**.

This study aimed to simulate the fluid flow arising from the capillary action in a porous channel. To this end, the effect of geometric and physical parameters on capillarity and fluid flow was investigated. Geometric parameters involved

both channel dimensions and pore dimensions, whereas the physical parameters were fluid physical properties such as viscosity, surface tension coefficient (STC), and CA.

1.1.1. Washburn's model for fluid imbibition through the capillary action

The passive fluid flow mechanism in the paper is due to the capillary force within the fluid and paper fibers and is known as capillary flow [5]. Thus, the fluid wicks through the paper by the capillary action with no need for external pumps [20]. The interaction of the paper and fluid develops the two types of cohesive and adhesive forces in opposite directions. When the paper and fluid are in contact, the interaction between fluid molecules is cohesive force, while the interaction between fluid and substrate molecules is called adhesive force [11, 13, 20].

The adhesive force causes spreading of fluid through the paper, whereas the cohesive force (i.e., surface tension) minimizes the surface area of the fluid. Therefore, the fluid flow occurs when the adhesive force overcomes the cohesive force [20]. In other words, the force difference between two sides of the meniscus (the developed interfacial curvature in the wicking fluid, **Fig. S1**) creates a pressure gradient leading to the fluid flow [5, 11]. This pressure drop is called the capillary or Laplace pressure and is obtained through the Young-Laplace equation:

$$P = -\sigma\left[{}^{1}/_{R_1} + {}^{1}/_{R_2}\right] \qquad (1)$$

R_1 and R_2 are the maximum and minimum radius of curvature in different phases, and σ is the STC of the fluid at a specific temperature. For a circular microchannel with a radius of R_c, the capillary pressure is obtained through the following equation [12, 20]:

$$P = -2\sigma cos\theta / R_c \qquad (2)$$

θ (contact angle) is the angle between the meniscus and the wall. It is the wettability characteristic of the solid wall.[11] When $\theta < 90^{\circ}$, the surface is wettable, and the curvature is of a concave shape. In contrast, when $\theta > 90^{\circ}$, the surface is non-wettable with the fluid, and the curvature is of a convex shape.

Since most of the microchannels are rectangular, to estimate the R_c, the hydraulic radius is defined as the follows [11, 18, 19, 22, 23]:

$$P = -2\sigma cos\theta / R_h \qquad (3)$$

By replacing $R_h = \frac{A}{P} = \frac{wh}{2(w+h)}$ (w and h are the width and height of the rectangular microchannel, respectively):

$$P = -4cos\theta\left({}^{1}/_{w} + {}^{1}/_{h}\right) \qquad (4)$$

According to the Navier-Stokes equations (conservation of mass and momentum equations):

$$\nabla.\vec{v} = 0 \qquad (5)$$

$$-\nabla P + \mu\nabla^2\vec{v} + \rho\vec{g} = \rho\left[{}^{\partial v}/_{\partial t} + (v.\nabla)v\right] \qquad (6)$$

Where ∇P is the pressure gradient representing the capillary pressure, $\mu\nabla^2\vec{v}$ represents the viscous forces, $\rho\vec{g}$ represents the gravity forces, and the right-side term is inertia. Washburn's assumptions are as follows [5, 13, 24]:

1. The flow is continuous, steady, fully developed, and along the length of the channel.

2. The Reynolds number, which is the relation of inertia to the viscosity, is low; therefore, the flow is laminar ($Re = \rho v D_h/\mu$).
3. The cross-section of the channel is constant.
4. The fluid is Newtonian ($\mu = const.$), and the flow is incompressible ($\rho = const.$).
5. The dimensionless capillary number is low; thus, the Ca is constant ($Ca = \mu V/\sigma \ll 1$).
6. There is a no-slip condition on the walls.
7. The pressure gradient is linear and is related to time.
8. The dimensionless Bond number is low so that the gravity can be neglected compared to surface tension ($Bo = \rho g D_h^2/\sigma$).
9. The swelling effect of the paper fibers is not considered.

Based on the above assumptions, the effect of inertia and gravity is neglected, and Washburn's equation is achieved as below:

$$x = \sqrt{{\sigma cos\theta}/{2\mu}\, R_c t} \qquad (7)$$

Where x is the wetted length (the length that the fluid was wicked), σ, θ, and μ are the wicking fluid STC, CA, and viscosity, respectively. R_c is the capillary radius (which equals the hydraulic radius of the microchannel), and t is the imbibition time of the fluid through the microchannel [18–20, 25].

1.1.2. Darcy's law for fluid flow in a porous structure

Henry Darcy, in 1856 found a linear relationship between the fluid flow and pressure gradient in a porous medium through his experiments ($Q = {kA}/{\mu}\,{\Delta P}/{L}$).[16, 19] Considering $v = {Q}/{A}$ and $\nabla P = {\Delta P}/{L}$, we have the equation as below:

$$v = -{k}/{\mu \nabla P} \qquad (8)$$

Where k is the permeability of the porous media and means how easily liquid can pass through the substrate. Permeability is an important characterstic for a porous structure and represents the possibility of fluid transition from the structural pores [11, 13, 20]. v, μ, and ∇P are the average fluid velocity, fluid viscosity, and pressure gradient, respectively.

Regarding Darcy's equation, the dimension of permeability is [m^2]. Permeability can be calculated experimentally. It has various relations according to the conditions of the experiments performed by different researchers [8, 9, 14, 20]. Although many researchers have investigated permeability, there is no specific equation or model for the paper substrate [5]. Therefore, achieving a relationship for permeability was another aim of the present study. Considering the assumptions for Darcy's law, the wetted-length equation is as below [8, 11, 13, 24, 25]:

$$x^2 = -{2k}/{\mu}\,\Delta P_c t \qquad (9)$$

The negative sign represents that the direction of the flow is from the higher pressure to the lower one. Darcy's assumptions are as follows [5]:

1. The flow in the porous medium is continuous, developed, and laminar.
2. Fluid velocity has linear behavior with the pressure gradient.
3. The fluid has a constant viscosity and CA, and the fluid is incompressible.
4. The pressure gradient is linear in the x-direction and is constant over time.
5. The effect of hydrostatic and atmospheric pressures is neglected compared to the surface tension effect.

1.1.3. Equations in the present study

Songok et al. found that there is a power-law relation between the wetted length and time in a paper substrate ($x = at^b$) [3]. Considering this relationship and assuming paper as a porous structure made of bundles of capillary fibers and investigating various simulation parameters, a modified equation can be obtained, as explained in Section

Fig. 13 a) Negative correlation of fluid imbibition and fluid viscosity **b)** More pressure drop by increasing viscosity

3.4. Proposing and evaluating a modified Washburn's equation

This study investigated fluid flow by capillary action in the paper substrate with orderly (non-random) pores. The effect of geometrical and physical parameters on the wetted length and average pressure was evaluated, and the consistency of the present and a recent study [21] was verified by comparing wetted-length results, Section **Fig. 2** The wetted length diagrams in different element sizes

3.2. Verification and validation of the simulation model.

According to the simulations, variation in physical parameters such as STC increase, CA decrease, and viscosity decrease leads to increasing pressure gradient and fluid imbibition. Therefore, the effect of physical parameters on the capillary pressure was verified as expressed in Washburn's model. Considering different simulations, the wetted length in the present study can be proposed as below:

$$x \propto {}^{1}/_{R_h} \sqrt{WH\sigma L\varepsilon cos\theta/\mu} \qquad (10)$$

Where R_h is the pore hydraulic radius, W, H, and L are the channel dimensions (width, height, and length, respectively), ε is the porosity fraction, σ is the STC, θ is the fluid CA on the surface, and μ is the fluid viscosity. Considering a constant value, the modified Washburn's equation is as follows:

$$x = {}^{\alpha}/_{R_h} \sqrt{{}^{WHL\varepsilon cos\theta}/_{\mu}} \qquad (11)$$

Where α is a constant value and can be calculated through experimental methods [14] and $\alpha = 1.2$ for the present study. By comparing Eq. 11 with Darcy's equation (*Eq. 9*), the permeability is as below:

$$k = -WHL\varepsilon/128\alpha R_h \qquad (12)$$

Fig. 14 shows the consistency of results obtained from modified Washburn's equation, simulation and Schaumburg and Berli's study.

Fig. 14 Consistency of the modified Washburn's equation with this simulation and a recent study

4. Conclusion.

2. Materials and methods

2.1. Software and solution simulation

The volume of fluid (VOF) multiphase modeling in ANSYS fluent v19.1 was utilized for the numerical simulation. The VOF multiphase modeling can trace and analyze the interface of two or more immiscible fluids. In this model, the volume fraction of each fluid is traced. Investigating the fluid flow in the liquid and air interfaces was the reason for this modeling in the present study. Curve Expert Professional 1.6.5 (Hyams Development) was also utilized to predict the wetted length vs. time equation.

2.2. Geometry of the porous structure

Geometry was designed in AutoCAD 2019 (Autodesk, United States). The paper was assumed to have orderly or non-random pores; therefore, the pores were cubic, and the cubes were interconnected in the flow direction through a quarter of one face. As can be observed from **Fig. 1a**, the fluid flow is parallel to the direction of pores. The dimension of each pore was 10 μm according to field emission scanning electron microscopy (FESEM) images (**Fig. S2**), and the channel had the length, width, and thickness of 500, 1000, and 100 μm, respectively. The porous structure had a porosity of 0.25. These dimensions were utilized only for validation. Due to heavy computations, a smaller length of the channel (100 μm) was assumed for further analysis (**Table S2**).

2.3. Initial and boundary conditions

The initial wetted length was assumed to be 5 μm, and no-slip condition was considered for all walls. The CA between the surface of the pores and fluid was lower than 90º (**Fig. S3**); therefore, fluid could pass from one pore to the next through the interface. The inlet and outlet of the paper channel were exposed to atmospheric pressure. The top, bottom, and lateral walls had different CAs considering the type of modeling (**Fig. 1a-d**, **Fig. S5**). The results of all the

simulations were compared with the reference model simulation. The properties of the reference model are shown in **Table S2**.

Fig. 1 a) Isometric view of the proposed paper-based channel and different walls **b)** Side view of the channel and initial wetted length of 5 µm **c)** More precise view of two interconnected pores, surfaces colors with blue lines have

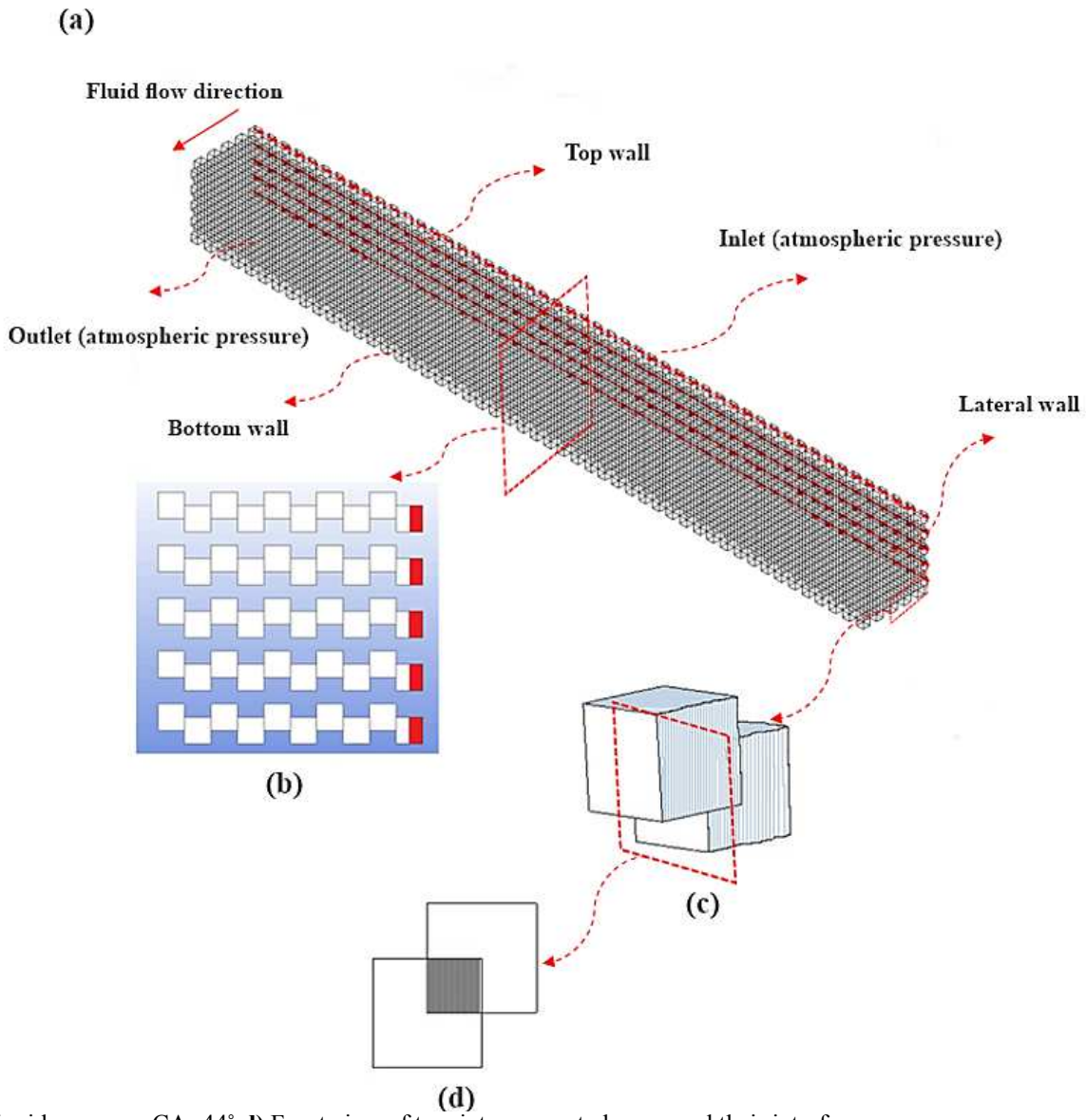

liquid-on-paper CA=44˚ **d)** Front view of two interconnected pores and their interface

2.4. Mesh independence study

The automatic meshing method (triangular) of the ANSYS fluent with different element sizes was used to achieve mesh independency. The simulation time and computations increased by decreasing the element size, nodes, and elements. The element sizes of 2.5, 5, 7.5, and 10 µm were evaluated. The meshing quality was determined by the aspect ratio, orthogonal quality, and skewness parameters. Since the aforementioned element sizes were in the

appropriate range of the qualification determinants, the wetted-length plot was another way of evaluating the mesh independency.

2.5. The method of achieving diagrams

The wetted length over time and average pressure over the channel length diagrams were introduced. The wetted length was achieved through the volume fraction function along the flow direction in a plane (named plane 1 and shown in **Fig S4**). For the pressure over the channel length diagram, the average pressure in the final time was obtained every 5 µm along the flow direction. This plot indicated pressure variations before and after the meniscus.

2.6. The effect of geometric and physical parameters

The effect of geometric and physical parameters was investigated, and the wetted length and pressure results were analyzed and compared with the reference model. Geometric parameters involved the geometry and dimensions of the pore, channel dimensions, and porosity. The investigated physical parameters are CA, STC, and viscosity. The variations of these parameters in different simulations are displayed in **Table S3**.

3. Results

3.1. Mesh independency study

According to the wetted length over time diagram (**Fig. 2**), the wetted length diagrams in different element sizes were approximately equal. The element size of 5 µm was chosen due to the smoother wetted-length curve.

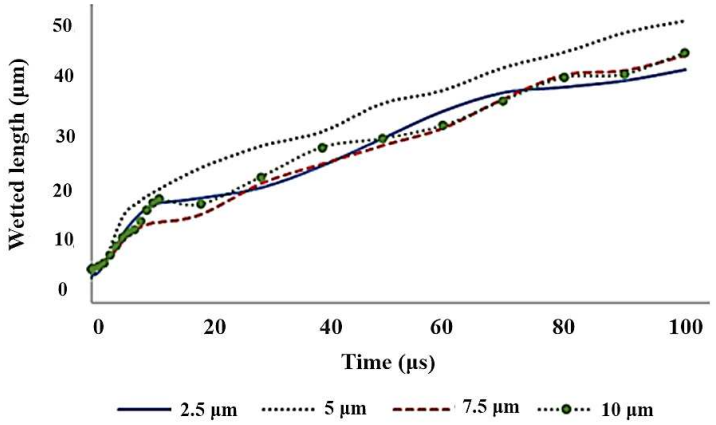

Fig. 2 The wetted length diagrams in different element sizes

3.2. Verification and validation of the simulation model

This simulation aimed to explain the diagrams and validate the modeling by comparing them with other studies. The fluid wicking through the capillary action was simulated for a 500×1000×100 μm^3 channel whose walls (top, bottom, and lateral) had the CA of adhesive tape (CA=78˚). The results of the wetted length and pressure are presented in **Fig. 3**. The schematic picture of the fluid position and average pressure at the beginning and the end of the simulation is shown in **Fig. 3a-f**. Because of more CA on the lateral walls and consequently less hydrophilicity and capillarity, the fluid wicked more in the middle of the channel (**Fig. 3a-d**). Lower average pressure is also observed in interface according to the liquid and air existance (**Fig. 3e,f**).

According to **Fig. 3g**, the slop of the wetted-length diagram and consequently the fluid velocity decreased over time. In fact, the liquid wicked into the channel with high speed at the beginning due to confronting a massive hydrophilic surface and, then, its velocity decreased over time due to increasing the wetted length, channel filling, and resistance. A diagram of average pressure over the channel length is illustrated in **Fig. 3h**. A pressure drop in the liquid zone suggested that the capillary flow occurred from the higher pressure to the lower. After the meniscus position, the average pressure increased to the atmospheric pressure due to the air phase and the outlet boundary conditions. According to **Fig. 3h**, the minimum of the plot is the position of the liquid and air interfaces (meniscus). Schaumburg and Berli solved equations for a multilayer paper and investigated the effect of different parameters such as gravity and inlet volumes on wetted length [21]. The present research findings are consistent with Schaumburg and Berli's results by comparing the wetted-length diagrams for a more extended period (**Fig. 3i**).

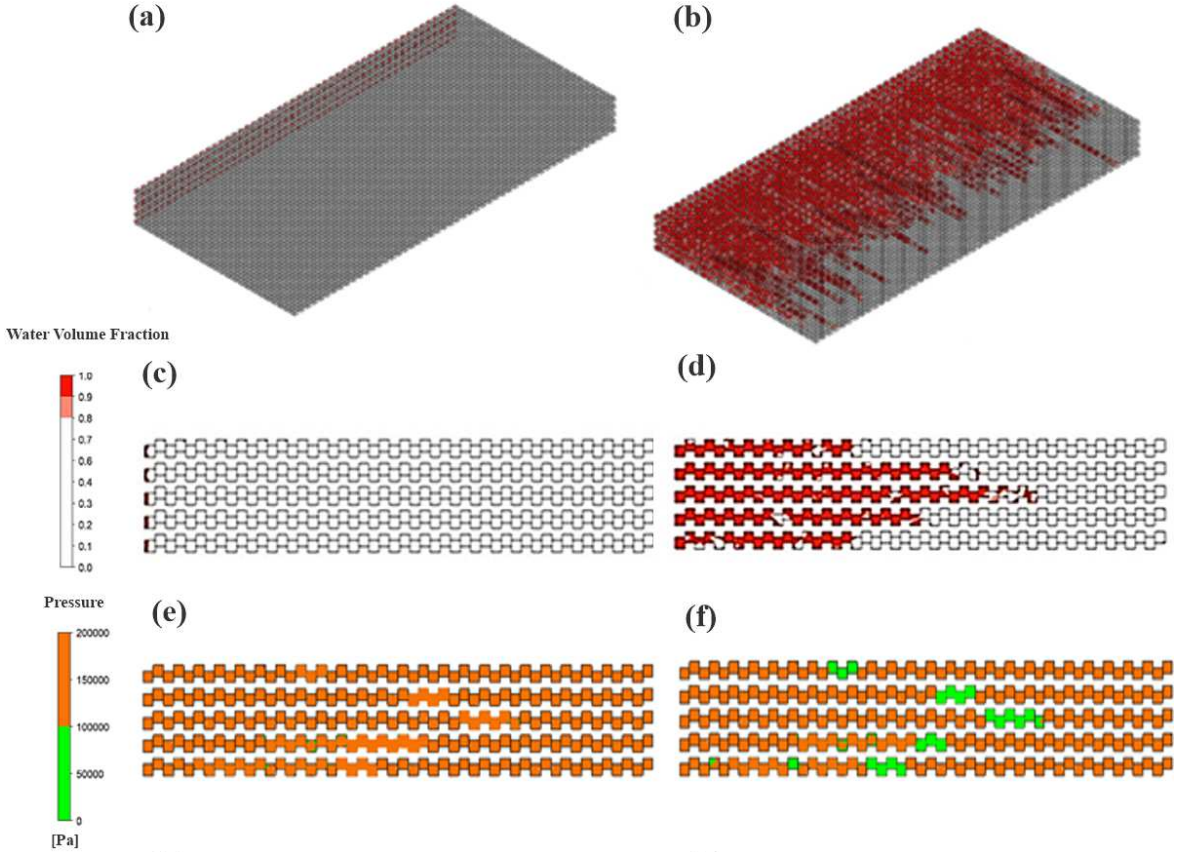

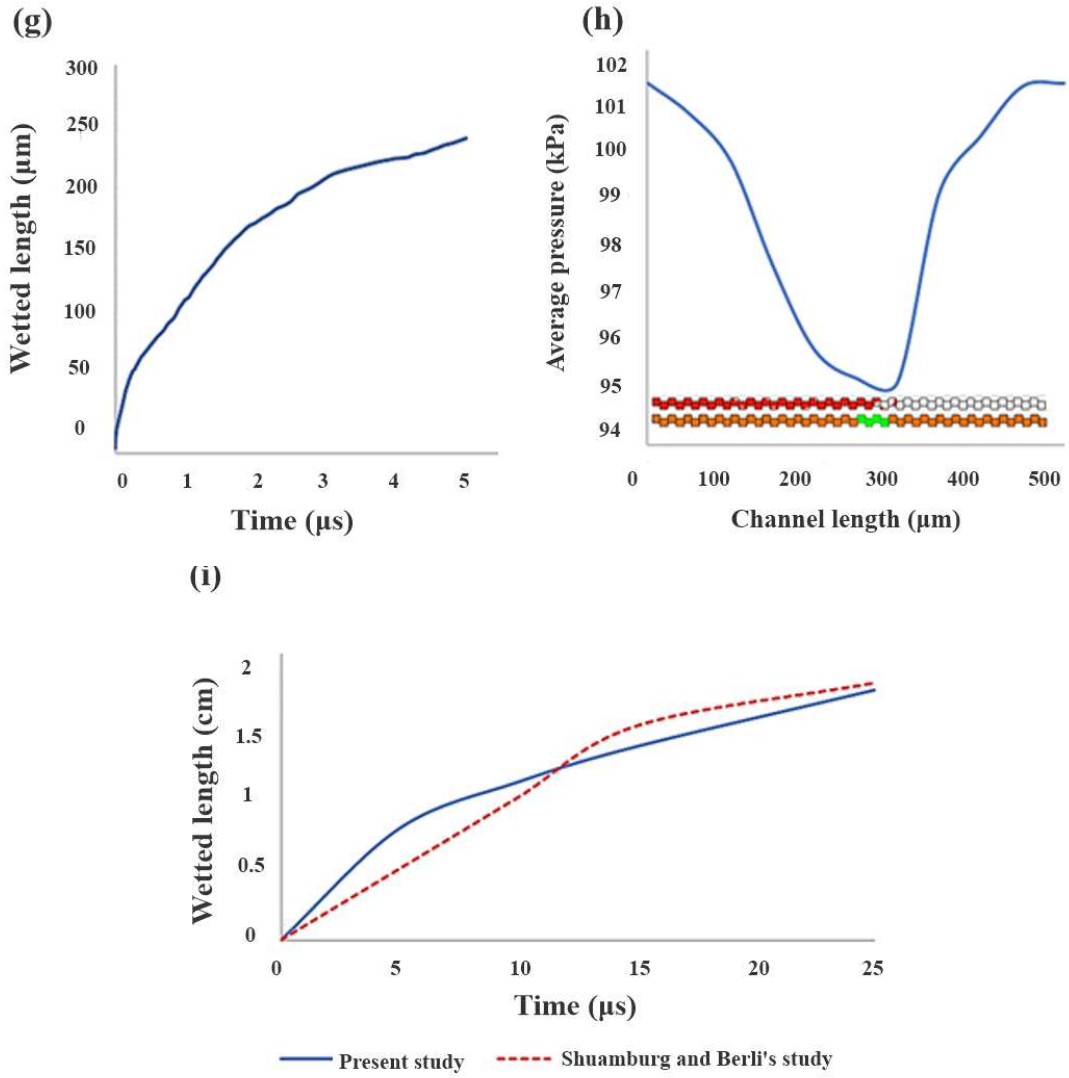

Fig. 3 Isometric view of the wetted length **a)** at the initial time (0 ms), **b)** after 5 ms, **c)** The wetted length at the initial time (0 ms) in plane 1, **d)** Wetted length after 5 ms in plane 1, the red color assigns for the liquid phase, **e)** Average pressure at initial time (0 ms) in plane 1, **f)** Average pressure after 5 ms in plane 1, **g)** Wetted length over time diagram, more wetted-length variations at the beginning of the flow due to lower resistance, **h)** Average pressure-channel length diagram, pressure drop before meniscus in the presence of liquid phase, and **i)** Consistency of wetted length in the present study and Schaumburg and Berli's study

3.3. The effect of various parameters

3.3.1. Boundary condition effect

Four types of boundary conditions were defined (5th row in **Table S3, Fig. S5**). As depicted in **Fig. 4a**, the wetted length when 4 boundaries are hydophlic walls (4BH) was more than the other boundary conditions due to owning more capillary surfaces and more capillary force. According to the average pressure-channel length diagram (**Fig. 4b**),

the pressure drop was also more in 4BH because of more capillary surfaces. Moreover, pressure fluctuations in the liquid phase were observed due to the interfacial cross-section's alteration perpendicular to the fluid flow. The interface of every two interconnected pores had a smaller cross-section (**Fig. 4c**), and when the fluid flowed over that interface, the velocity must be increased based on the mass conservation law ($Q_1=Q_2$, $A_1v_1=A_2v_2$). Therefore, according to Bernoulli's equation, any velocity decrease results in a pressure increase when gravity is constant. The average pressure tended to decrease along the channel in the liquid zone. Still, when the fluid passed the interface (e.g., after 10 µm), the cross-section became larger and led to a decrease in velocity and an increase in the pressure.

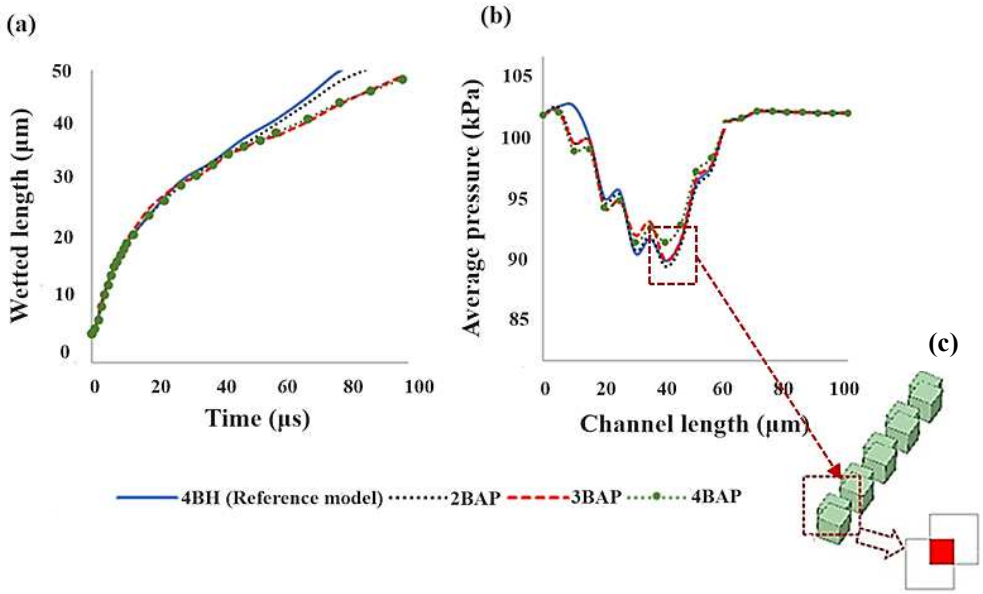

Fig. 4 a) More capillary force in 4BH due to having more capillary surface, **b)** More pressure drop when the capillary surface was more. The pressure fluctuations can be observed after every pore interface, (4BH: 4 boundaries are hydrophilic, 2BAP: 2 boundaries are exposed to atmospheric pressure, 3BAP: 3 boundaries are exposed to atmospheric pressure, 4BAP: 4 boundaries are exposed to atmospheric pressure), and **c)** Cross-section decrease in the interface of two interconnected pores, and velocity decrease and pressure increase according to Bernoulli's equation

3.3.2. Effect of pore geometry

The capillary effect was investigated for the three cubic, cylindrical, and spherical pore geometries with the same hydraulic radius. The wetted length was more when the pore geometry was cubic; the other geometries had almost equal wetted lengths (**Fig. 5a**). The capillary surface could be a reason for this phenomenon. As depicted in **Fig. 5b**, the average pressure variation was more when the pore geometry was cubic. The main reason for more pressure drop in the cubic pore was the trapping of air in the edges of the pore. Therefore, the pressure drop increased to push the fluid forward. The pressure fluctuations due to cross-section alterations, expressed in Section 3.3.1. Boundary condition effect were also observed. The surface which has a CA lower than 90° and causes capillary action was called the capillary surface. The surfaces of pores and channel walls were examples of the capillary surface. However, in this study, the capillary surface was used to differentiate between the channel walls and hydrophilic pore surfaces, and

the term capillary surface was only applied for the hydrophilic pore surfaces. The capillary surface is shown in **Fig. 5c** for two interconnected pores. By calculating the capillary surface for one pore in different geometries, it was realized that the capillary surface was more when the pore was cubic. Moreover, the Washburn's equation coefficients obtained from the wetted length vs. time diagram equaled the proportion of capillary surfaces in different pore geometries (See **Table S4** for more details.).

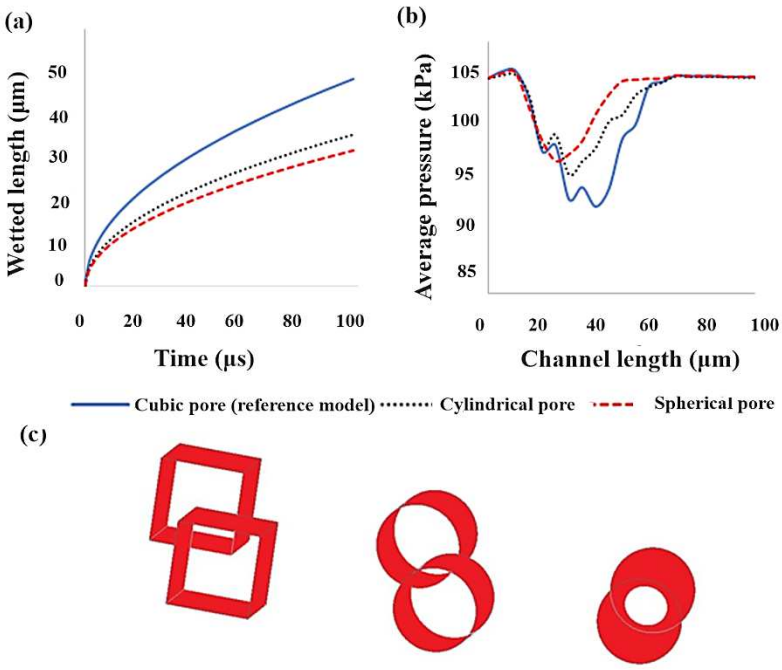

Fig. 5 a) More fluid imbibition because of more capillary surface in cubic geometry, **b)** More pressure variations along the channel owing to the air trap in cubic pore modeling, and **c)** Capillary surfaces for two interconnected pores demonstrated in red color in the cubic, cylindrical , and spherical pores

3.3.3. Effect of pore size variation

Simulations were performed for the pore width of 5, 10, and 20 µm to investigate the effect of pore dimensions on the wetted length and pressure. As discussed before, 10 µm is the reference size. According to the wetted length over time diagram (**Fig. 6a**), halving or doubling the width of the pore had a similar effect on the wetted length, and the fluid imbibition was lower than the reference model. The pressure variation is illustrated in **Fig. 6b**. The pressure drop in the 5 µm pore width was more than the other two (10 and 20 µm) due to the presence of more considerable resistance and more pressure drop to push the fluid forward. Twenty µm pore width compared to 10 µm had less resistance but required more pressure drop to compensate for the lower capillary surface. Therefore, more pressure drop was observed for the 20 µm pore width.

Achieving the same wetted length in 5 and 20 µm widths can be for two reasons: capillary surface and channel resistance. The capillary surface was described before and can be calculated accordingly. The porosity was the same

in all the geometries; so, the number of pores in smaller pore width was more than the larger one. The channel resistance is calculated using Poiseuille's law, and is inversely proportional to the fourth power of the hydraulic radius ($\propto \frac{1}{r_h^4}$). The capillary surface and channel resistance are calculated in **Table S5**. According to **Table S5**, the smaller pore width had more capillary surface and more channel resistance. The capillary surface helped fluid wicking, whereas the channel resistance prevented capillarity. Thus, increasing or decreasing the pore width had the same effect on the wetted length.

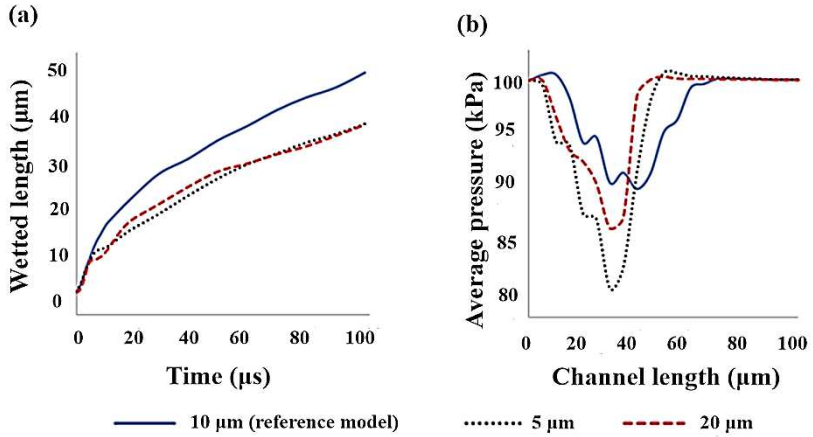

Fig. 6 a) Liquid imbibition length **b)** Pressure drop in different pore widths

3.3.4. Effect of channel width

The channel widths of 0.5 and 1 mm were investigated. According to **Fig. 7a**, the wetted length in 1 mm channel was more because of more capillary surfaces. The average pressure measurements along the channel are depicted in **Fig. 7b**. More pressure drop in 0.5 mm channel width modeling was observed. This geometry had a few capillary surfaces; so, the pressure drop should be increased to lead the fluid to penetrate forward. The pressure diagram for the wider channel shifted slightly right because it had a higher wetted length. By comparing the ratio of the wetted-length equation obtained from the diagram and the proportion of the channel width (**Table S6**), it was observed that the equation coefficient changed by the square root of the channel width ratio ($x \propto \sqrt{W}$).

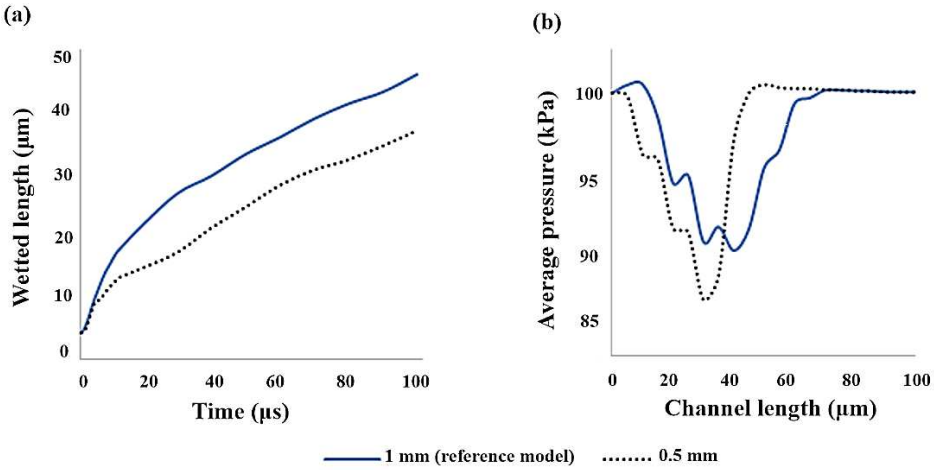

Fig. 7 a) More wetted length in the wider channel due to more capillary surface **b)** More pressure drop in smaller channel owing to the less capillary surface

3.3.5. Effect of the channel height

Two geometries of 50 and 100 µm channel height (thickness) were simulated. As illustrated in **Fig. 8a**, the liquid phase could wick more in the thicker channel because of more capillary surface presence. According to the pressure diagram (**Fig. 8b**), the pressure drop in the thinner channel was more because fewer capillary surfaces required more pressure to activate the fluid flow. The pressure diagram for the thicker channel shifted slightly right because it had a more wetted length. As shown in **Table S7**, the wetted length over time by channel heights variation demonstrated that the equation coefficient changed proportionally to the square root of the channel heights ($x \propto \sqrt{H}$).

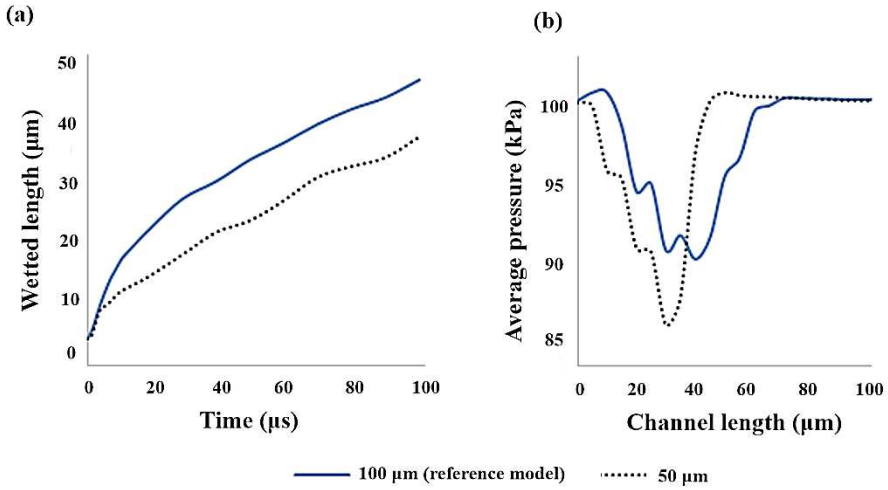

Fig. 8 a) More fluid imbibition in the thicker channel because of the more capillary surface **b)** More pressure drop in the thinner channel

3.3.6. Effect of channel length

The channel lengths of 50 and 100 µm were modeled. This simulation aimed to investigate the effect of channel length on the wetted length and pressure gradient. According to the wetted-length diagram (**Fig. 9a**), the fluid imbibition increased by a channel length increase. It can be hypothesized that the longer channel can create more pressure gradients. The pressure drop in the shorter channel was also more (**Fig. 9b**). By comparing the ratio of the coefficients and the length changes (**Table S8**), the coefficients were changed concerning the square root of the length change ($x \propto \sqrt{L}$).

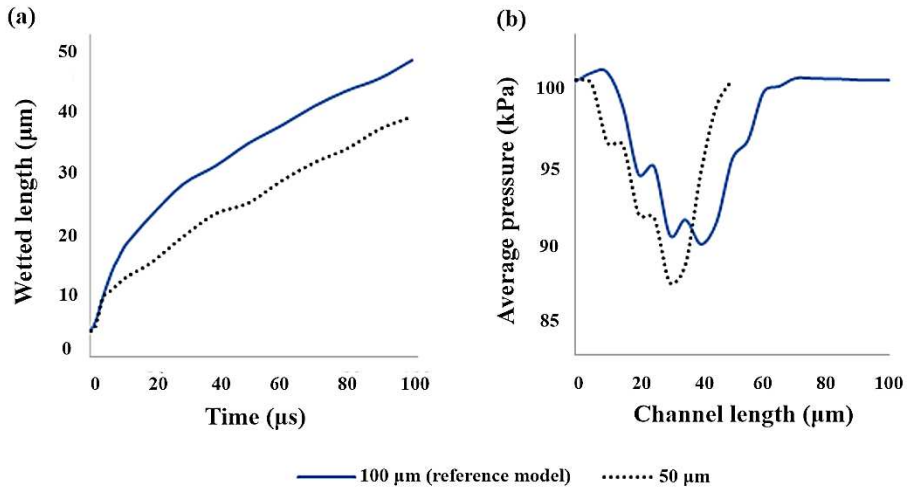

Fig. 9 a) More fluid imbibition in the longer channel **b)** More pressure drop in 50 µm channel length

3.3.7. Effect of the porosity

The porosities of 0.125 and 0.25 were evaluated. According to **Fig. 10a**, the wetted length in the porosity of 0.25 was more because of more capillary surfaces. The average pressure along the channel is illustrated in **Fig. 10b**. The pressure drop in lower porosity was more owing to having a less capillary surface and requiring more pressure drop to push the fluid forward. In the porosity of 0.25, the pressure diagram shifted slightly right because of more fluid imbibition. According to **Table S9**, the wetted-length coefficient of the equation has a positive correlation with the square root of the porosity ($x \propto \sqrt{\varepsilon}$).

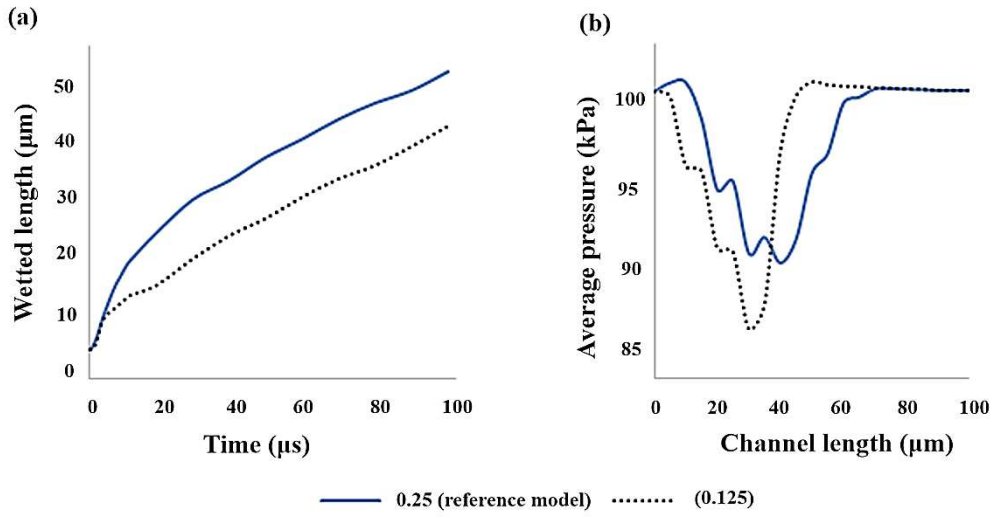

Fig. 10 a) More liquid wicking when porosity was more **b)** Pressure drop in the porosity of 0.125 due to having fewer capillary surfaces

3.3.8. Effect of CA variations

The effects of CA of 22°, 44°, and 66° were investigated. According to **Fig. 11a**, the wetted length increased by decreasing the CA. Lower angles for fluid on a surface meant more hydrophilicity and, therefore, more capillary. Thus, lowering the CA caused more fluid imbibition. According to **Fig. 11b**, a decrease in CA resulted in more pressure drop because lower CAs created more capillary action due to having more hydrophilicity. In other words, decreasing CA meant increasing the cosine of CA ($x \propto \sqrt{\cos CA}$) and the pressure gradient in the capillary pressure equation (**Table S10**).

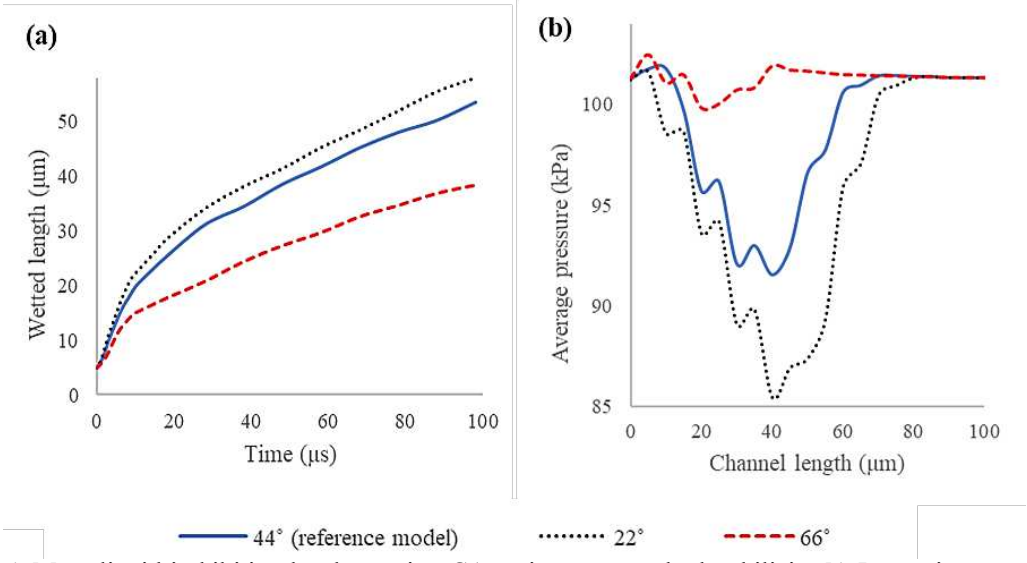

Fig. 11 a) More liquid imbibition by decreasing CA owing to more hydrophilicity **b)** Increasing pressure drop by reduction of the CA

3.3.9. Effect of the surface tension coefficients

The STCs of 0.0364, 0.0728, and 0.1564 N/m were considered for the liquid phase. According to **Fig. 12a**, the wetted length increased by raising the STC. According to the capillary pressure equation, the STC was positively correlated with the capillary pressure and the fluid imbibition. More pressure drop was also observed with a higher STC (**Fig. 12b**). According to the capillary pressure equation, the capillary pressure and, therefore, wetted length were directly proportional to the STC and the square root of the STC ($x \propto \sqrt{\sigma}$), respectively (**Table S11**).

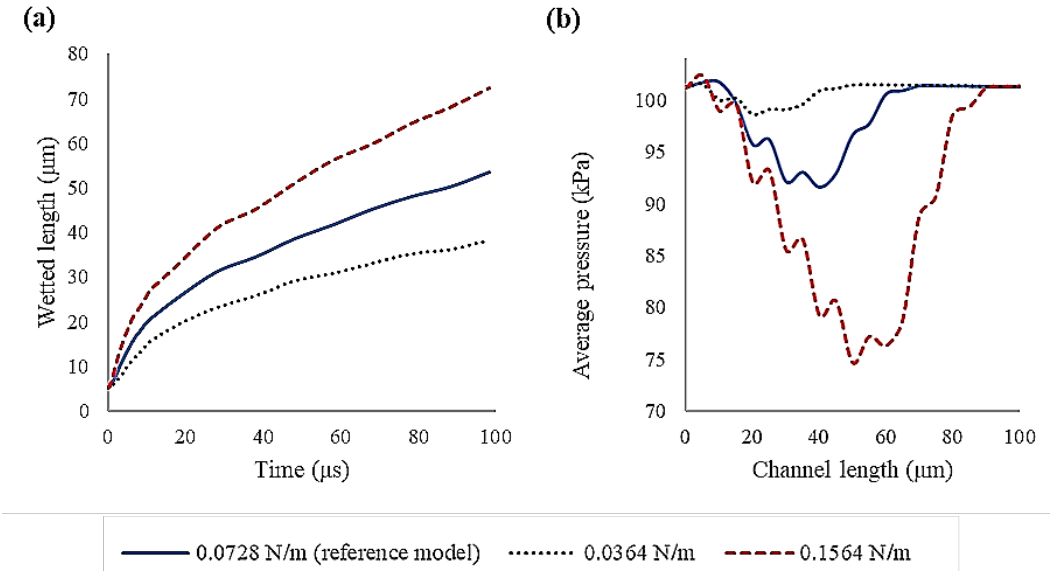

Fig. 12 a) Increasing fluid penetration by increasing the STC **b)** More pressure drop by increasing the STC.

3.3.10. Effect of the fluid viscosity

The fluid viscosity for water in 25°C, half and double, was considered. As depicted in **Fig. 13a**, more fluid viscosity resulted in a lower wetted length because of more flow resistance. Moreover, the viscosity was negatively correlated with the capillary pressure and the fluid imbibition in the capillary pressure equation. The higher viscosity created more flow resistance and pressure drop (**Fig. 13b**). According to **Table S12**, the wetted length was inversely proportional to the square root of the fluid viscosity ($x \propto \sqrt{1/\mu}$).

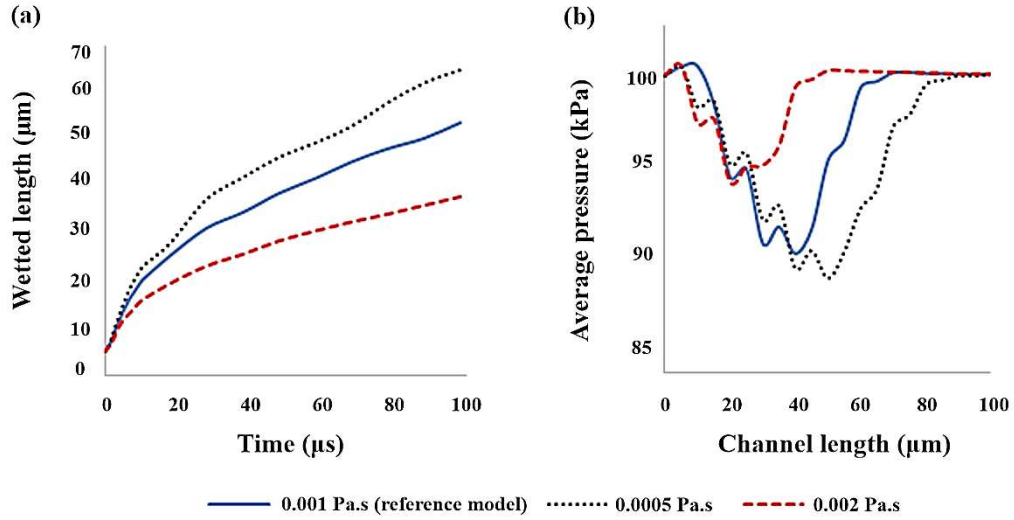

Fig. 13 a) Negative correlation of fluid imbibition and fluid viscosity **b)** More pressure drop by increasing viscosity

3.4. Proposing and evaluating a modified Washburn's equation

This study investigated fluid flow by capillary action in the paper substrate with orderly (non-random) pores. The effect of geometrical and physical parameters on the wetted length and average pressure was evaluated, and the consistency of the present and a recent study [21] was verified by comparing wetted-length results, Section **Fig. 2** The wetted length diagrams in different element sizes

3.2. Verification and validation of the simulation model.

According to the simulations, variation in physical parameters such as STC increase, CA decrease, and viscosity decrease leads to increasing pressure gradient and fluid imbibition. Therefore, the effect of physical parameters on the capillary pressure was verified as expressed in Washburn's model. Considering different simulations, the wetted length in the present study can be proposed as below:

$$x \propto {}^{1}/_{R_h} \sqrt{WH\sigma L\varepsilon cos\theta/\mu} \qquad (10)$$

Where R_h is the pore hydraulic radius, W, H, and L are the channel dimensions (width, height, and length, respectively), ε is the porosity fraction, σ is the STC, θ is the fluid CA on the surface, and μ is the fluid viscosity. Considering a constant value, the modified Washburn's equation is as follows:

$$x = {}^{\alpha}/_{R_h} \sqrt{{WHL\varepsilon cos\theta}/{\mu}} \qquad (11)$$

Where α is a constant value and can be calculated through experimental methods [14] and $\alpha = 1.2$ for the present study. By comparing Eq. 11 with Darcy's equation (*Eq. 9*), the permeability is as below:

$$k = -WHL\varepsilon/128\alpha R_h \qquad (12)$$

Fig. 14 shows the consistency of results obtained from modified Washburn's equation, simulation and Schaumburg and Berli's study.

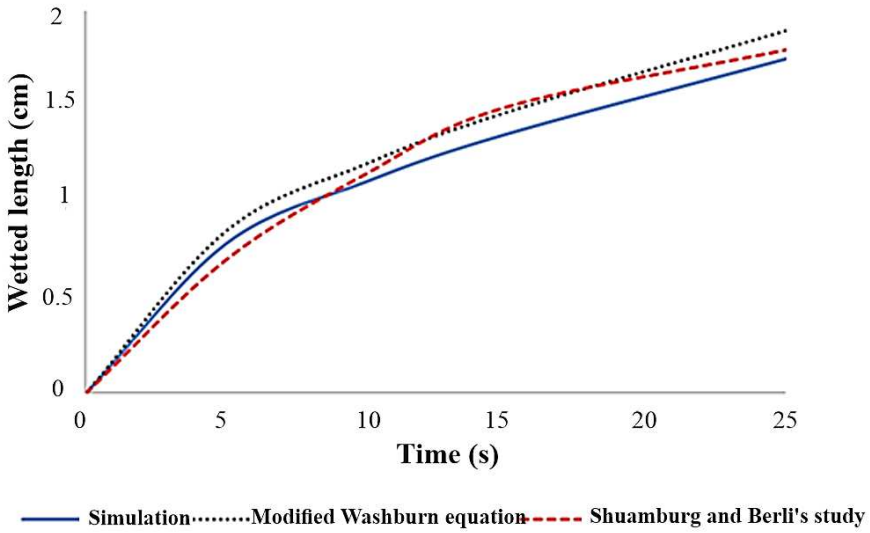

Fig. 14 Consistency of the modified Washburn's equation with this simulation and a recent study

4. Conclusion

According to the wetted length over time diagram, the fluid wicked very fast at the beginning of the flow (high slope of the diagram), the fluid velocity slowed down, and the wetted length reached a constant value in the final period. Such a behavior was because of filling the pores near the inlet and increasing the flow resistance. In the diagram of average pressure along with the channel, a pressure drop was observed in the fluid phase suggesting that the capillary action leads to a pressure gradient and fluid imbibition [5, 8, 20]. The pressure fluctuations were also perceived owing to cross-section alterations that changed the velocity (conservation of mass law) and pressure (Bernoulli's equation). Changing the geometric parameters did not directly affect the capillary pressure, whereas wetted length and pressure alterations were observed. Capillary surface and channel resistance were the factors which were investigated in this study. The pore surfaces and channel walls were capillary surfaces in this simulation. Here, the capillary surface is hydrophilic (CA<90°), and the capillary action that occurs through this surface helps fluid wicking. The channel resistance was obtained through Poiseuille's equation. A decrease in capillary forces and wetted length was observed when the resistance increased. Changing geometric parameters such as pore size and porosity could change both capillary surfaces and fluid resistance or one of the aforementioned factors.

Supplementary material

See the supplementary material for the complete structure of this study.

Statements and Declarations

The authors declare that they have no known competing financial interests or personal relationships that could have appeared to influence the study reported in this paper.

Funding

This work was funded by University of Isfahan, Isfahan, Iran.

Competing interests

The authors have no relevant financial or non-financial interests to disclose.

Ethics approval (Not applicable)

This research does not contain any studies with human participants or animals performed by any of the authors.

Consent to participate (Not applicable)

This research does not contain any studies with human participants performed by any of the authors.

Consent for publication (Not applicable)

Availability of data and material

All useful data obtained during the study are available.

Authors' contributions

Samira Allameh was MSc. Student in biomedical engineering and she did this study as a master thesis under the supervision of Dr. Mohsen Rabbani. Samira wrote the manuscript and Mohsen modified and prepared it for publication.

References

1. Songok, J., Toivakka, M.: Enhancing capillary-driven flow for paper-based microfluidic channels. ACS Appl. Mater. Interfaces. 8, 30523–30530 (2016). https://doi.org/10.1021/acsami.6b08117
2. Baldwin, S.A., Van Bruggen, S.M., Koelbl, J.M., Appalabhotla, R., Bear, J.E., Haugh, J.M.: Microfluidic devices fitted with “flowver” paper pumps generate steady, tunable gradients for extended observation of chemotactic cell migration. Biomicrofluidics. 15, (2021). https://doi.org/10.1063/5.0054764
3. Songok, J., Tuominen, M., Teisala, H., Haapanen, J., Mäkelä, J., Kuusipalo, J., Toivakka, M.: Paper-based micro fluidics: Fabrication technique and dynamics of capillary-driven surface flow. ACS Appl. Mater. Interfaces. 6, 20060–20066 (2014). https://doi.org/10.1021/am5055806
4. Yuan, H., Chiu, P.Y., Chen, C.F.: Paper-based analytical devices for point-of-care blood tests. Biomicrofluidics. 15, 1–6 (2021). https://doi.org/10.1063/5.0055601
5. Walji, N.: Characterization of fluid flow in paper-based microfluidic devices, (2015)
6. Shay, T., Saha, T., Dickey, M.D., Velev, O.D.: Principles of long-term fluids handling in paper-based

wearables with capillary-evaporative transport. Biomicrofluidics. 14, (2020). https://doi.org/10.1063/5.0010417

7. Lee, W., Gonzalez, A., Arguelles, P., Guevara, R., Gonzalez-Guerrero, M.J., Gomez, F.A.: Thread/paper- and paper-based microfluidic devices for glucose assays employing artificial neural networks. Electrophoresis. 39, 1443–1451 (2018). https://doi.org/10.1002/elps.201800059
8. Elizalde, E., Urteaga, R., Berli, C.L.A.: Rational design of capillary-driven flows for paper-based microfluidics. Lab Chip. 15, 2173–2180 (2015). https://doi.org/10.1039/c4lc01487a
9. Liu, Z., Hu, J., Zhao, Y., Qu, Z., Xu, F.: Experimental and numerical studies on liquid wicking into filter papers for paper-based diagnostics. Appl. Therm. Eng. 88, 280–287 (2015). https://doi.org/10.1016/j.applthermaleng.2014.09.057
10. Nishat, S., Jafry, A.T., Martinez, A.W., Awan, F.R.: Paper-based microfluidics: Simplified fabrication and assay methods. Sensors Actuators, B Chem. 336, 129681 (2021). https://doi.org/10.1016/j.snb.2021.129681
11. Ashari, A.: Dual-Scale Modeling of Two-Phase Fluid Transport in Fibrous Porous Media, (2010)
12. Cito, S., Curto, J.P., Katakis, I.: Numerical and experimental study of flow and wall mass transfer rates in capillary driven flows in microfluidic channels, (2009)
13. Lagree, B.: Modelling of two-phase flow in porous media with volume-of-fluid method, (2014)
14. Cai, Q., Kooshapur, S., Manhart, M., Mundani, R.P., Rank, E., Springer, A., Vexler, B.: Numerical simulation of transport in porous media: Some problems from micro to macro scale. arXiv. 93, (2018). https://doi.org/10.1007/978-3-642-38762-3_3
15. Waghmare, P.R., Mitra, S.K.: A comprehensive theoretical model of capillary transport in rectangular microchannels. Microfluid. Nanofluidics. 12, 53–63 (2012). https://doi.org/10.1007/s10404-011-0848-8
16. Lade, R.K., Hippchen, E.J., Macosko, C.W., Francis, L.F.: Dynamics of Capillary-Driven Flow in 3D Printed Open Microchannels. Langmuir. 33, 2949–2964 (2017). https://doi.org/10.1021/acs.langmuir.6b04506
17. Sowers, T.W., Sarkar, R., Eswarappa Prameela, S., Izadi, E., Rajagopalan, J.: Capillary driven flow of polydimethylsiloxane in open rectangular microchannels. Soft Matter. 12, 5818–5823 (2016). https://doi.org/10.1039/c6sm00897f
18. Ichikawa, N., Hosokawa, K., Maeda, R.: Interface motion of capillary-driven flow in rectangular microchannel. J. Colloid Interface Sci. 280, 155–164 (2004). https://doi.org/10.1016/j.jcis.2004.07.017

19. Ichikawa, N., Maeda, R.: Interface motion driven by capillary action in circular and rectangular microchannel. Microscale Thermophys. Eng. 9, 237–254 (2005). https://doi.org/10.1080/10893950500196006

20. Kumar, S., Bhushan, P., Bhattacharya, S.: Fluid Transport Mechanisms in Paper-Based Microfluidic Devices. In: Paper Microfluidics: Theory and Applications. pp. 7–28. Springer (2019)

21. Schaumburg, F., Berli, C.L.A.: Assessing the rapid flow in multilayer paper-based microfluidic devices. Microfluid. Nanofluidics. 23, 1–10 (2019). https://doi.org/10.1007/s10404-019-2265-3

22. Zhu, Y., Petkovic-Duran, K.: Capillary flow in microchannels. Microfluid. Nanofluidics. 8, 275–282 (2010). https://doi.org/10.1007/s10404-009-0516-4

23. The Engineering Toolbox: Flow section channels, https://www.engineeringtoolbox.com/flow-section-channels-d_965.html

24. Saha, A.A., Mitra, S.K., Tweedie, M., Roy, S., McLaughlin, J.: Experimental and numerical investigation of capillary flow in SU8 and PDMS microchannels with integrated pillars. Microfluid. Nanofluidics. 7, 451–465 (2009). https://doi.org/10.1007/s10404-008-0395-0

25. Yadav, S., Sharma, N.N., Akhtar, J.: Paper for microfluidics: Selection criteria. AIP Conf. Proc. 2294, (2020). https://doi.org/10.1063/5.0031966

Figures

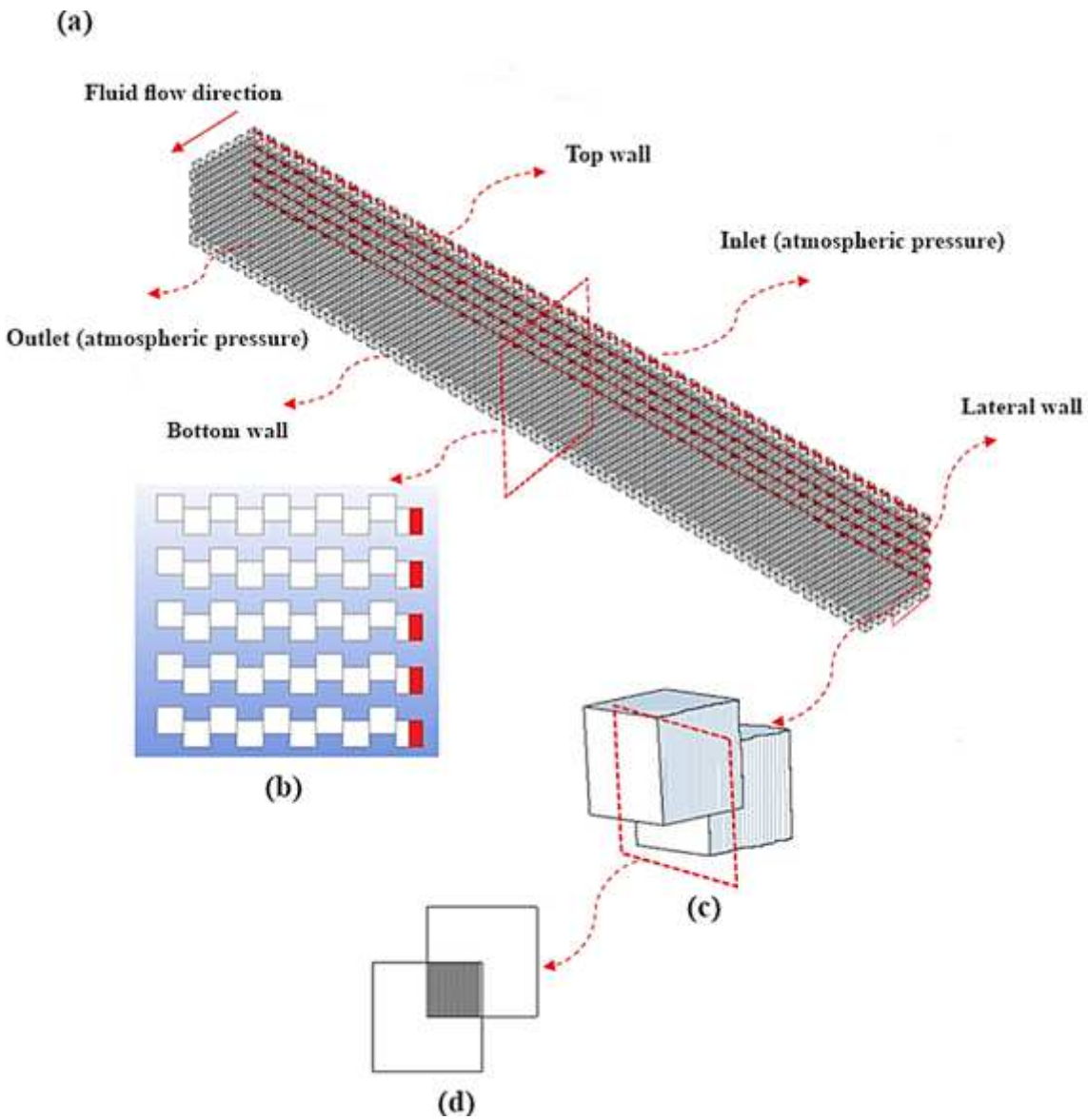

Figure 1

a) Isometric view of the proposed paper-based channel and different walls **b)** Side view of the channel and initial wetted length of 5 μm **c)** More precise view of two interconnected pores, surfaces colors with blue lines have liquid-on-paper CA=44˚ **d)** Front view of two interconnected pores and their interface

Figure 2

The wetted length diagrams in different element sizes

Figure 3

Isometric view of the wetted length **a)** at the initial time (0 ms), **b)** after 5 ms, **c)** The wetted length at the initial time (0 ms) in plane 1, **d)** Wetted length after 5 ms in plane 1, the red color assigns for the liquid phase, **e)** Average pressure at initial time (0 ms) in plane 1, **f)** Average pressure after 5 ms in plane 1, **g)** Wetted length over time diagram, more wetted-length variations at the beginning of the flow due to lower resistance, **h)** Average pressure-channel length diagram, pressure drop before meniscus in the presence of liquid phase, and **i)** Consistency of wetted length in the present study and Schaumburg and Berli's study

Figure 4

a) More capillary force in 4BH due to having more capillary surface, **b)** More pressure drop when the capillary surface was more. The pressure fluctuations can be observed after every pore interface, (4BH: 4 boundaries are hydrophilic, 2BAP: 2 boundaries are exposed to atmospheric pressure, 3BAP: 3 boundaries are exposed to atmospheric pressure, 4BAP: 4 boundaries are exposed to atmospheric pressure), and **c)** Cross-section decrease in the interface of two interconnected pores, and velocity decrease and pressure increase according to Bernoulli's equation

Figure 5

a) More fluid imbibition because of more capillary surface in cubic geometry, **b)** More pressure variations along the channel owing to the air trap in cubic pore modeling, and **c)** Capillary surfaces for two interconnected pores demonstrated in red color in the cubic, cylindrical , and spherical pores

Figure 6

a) Liquid imbibition length **b)** Pressure drop in different pore widths

Figure 7

a) More wetted length in the wider channel due to more capillary surface **b)** More pressure drop in smaller channel owing to the less capillary surface

Figure 8

a) More fluid imbibition in the thicker channel because of the more capillary surface **b)** More pressure drop in the thinner channel

Figure 9

a) More fluid imbibition in the longer channel **b)** More pressure drop in 50 μm channel length

Figure 10

a) More liquid wicking when porosity was more **b)** Pressure drop in the porosity of 0.125 due to having fewer capillary surfaces

Figure 11

a) More liquid imbibition by decreasing CA owing to more hydrophilicity **b)** Increasing pressure drop by reduction of the CA

Figure 12

a) Increasing fluid penetration by increasing the STC **b)** More pressure drop by increasing the STC

Figure 13

a) Negative correlation of fluid imbibition and fluid viscosity **b)** More pressure drop by increasing viscosity

Figure 14

Consistency of the modified Washburn's equation with this simulation and a recent study

Supplementary Files

This is a list of supplementary files associated with this preprint. Click to download.

- supplementarymaterialforsubmission.docx